1.E.3:
2.N

Nuclear Physics A293 (1977) 248–268; © *North-Holland Publishing Co., Amsterdam*

MAGNETIC MOMENTS OF $N = 50$ ISOTONES AND PROTON CORE POLARIZATION

O. HÄUSSER, I. S. TOWNER, T. FAESTERMANN †, H. R. ANDREWS, J. R. BEENE ††, D. HORN † and D. WARD

Atomic Energy of Canada Limited, Chalk River Nuclear Laboratories, Chalk River, Ontario, Canada K0J 1J0

and

C. BROUDE †††

The Weizmann Institute of Science, Rehovot, Israel

Received 1 July 1977

Abstract: Pulsed heavy-ion beams of ^{4}He, ^{6}Li, ^{32}S and ^{35}Cl have been used to populate isomeric states in $N = 50$ nuclei having a closed neutron shell and a rather pure $(p^{n}_{1/2}g^{n}_{9/2})$ proton configuration. The g-factors of the 3.4 μs $\frac{17}{2}^{-}$ state in ^{91}Nb, the 9.3 ns 11^{-} state in ^{92}Mo, the 10.1 μs $\frac{17}{2}^{-}$ state in ^{93}Tc, the 65.5 ns 6^{+} state and the 68 μs 8^{+} state in ^{94}Ru were measured for the first time and those of 8^{+} states in ^{90}Zr and in ^{92}Mo were remeasured with improved accuracy. The g-factors increase by $(4.2 \pm 0.8)\%$ as the $p_{1/2}$ proton subshell is filled and decrease by $(3.5 \pm 1.4)\%$ as the number of protons in the $g_{9/2}$ shell increases from two to four. Calculations that take core polarization into account in first-order perturbation theory explain quantitatively the observed magnetic moments. One-pion exchange current contributions have also been calculated.

E

NUCLEAR REACTIONS ^{88}Sr(^{4}He, 2nγ), ^{90}Zr(^{4}He, 2nγ), ^{92}Mo(^{4}He, 2nγ), E = 24–25 MeV; ^{88}Sr(^{6}Li, 3nγ), E = 34 MeV; ^{65}Cu(^{32}S, 2p2nγ), E = 120 MeV; ^{65}Cu(^{32}S, 3p2nγ), E = 132 MeV; ^{64}Ni(^{32}S, 2p2nγ), E = 132 MeV; ^{63}Cu(^{35}Cl, 2p2nγ), E = 120 MeV; measured $I_{\gamma}(\theta, H, t)$. ^{90}Zr, ^{91}Nb, ^{92}Mo, ^{93}Tc, ^{94}Ru deduced g-factors, $T_{1/2}$. Ge(Li) detectors. Enriched targets of ^{90}Zr, ^{65}Cu, ^{63}Cu, ^{64}Ni.

1. Introduction

The nuclear shell model, despite its spectacular success in explaining properties of nuclei near closed shells, nonetheless encounters some difficulty in accounting for magnetic properties of valence nucleons which deviate strongly from single-particle (Schmidt) values. The exchange of mesons between nucleons contributes to a shift in magnetic moments which is frequently ignored within the framework of the shell model. The existence of exchange moments has been recognized for a long time [1,2]), yet their role in heavy nuclei has only recently been explored [3,4]). Calculations of

† NRCC Postdoctoral Fellow.
†† Present address: Oak Ridge National Laboratory, Tennessee, USA.
††† Visiting Scientist at Queen's University, Kingston, Ontario, Canada during 1975–76.

exchange moments are somewhat uncertain because they depend sensitively on the interaction between nucleons at short range.

The truncation of the Hilbert space to a finite sized model space introduce a further error in standard shell-model estimates of magnetic moments. Small admixtures of core excited configurations can cause sizeable shifts of the magnetic moments [5-7]). Quantitative estimates of this core polarization effect requires knowledge of the appropriate particle-hole force and of energy differences between relevant particle-hole orbitals. Experimental information on the location and strength of M1 excitations in even-even nuclei can, in principle, determine the required parameters. Unfortunately, the available inelastic scattering experiments are not yet sufficiently conclusive to eliminate the theoretical uncertainties. In ^{90}Zr, for example, at most one third of the expected [8]) M1 strength has been identified in a recent (e, e') experiment [9]).

Core polarization contributions depend on the occupation number of valence shell nucleons and can thus be studied experimentally by observing g-factors of a series of nuclear states with a varying number of valence nucleons. Significant shifts in g-factors of isomeric $(h_{\frac{9}{2}})^n$ proton states in $N = 126$ isotones between ^{209}Bi and ^{214}Ra have recently been observed [10,11]). A theoretical interpretation of these results has been given by Towner *et al.* [7]).

We report here a similar study for $N = 50$ isotones between ^{90}Zr and ^{94}Ru. The present work expands considerably on previous measurements by Nagamiya *et al.* [12]) who observed substantial differences between the g-factors of 8^+ states in ^{90}Zr and ^{92}Mo, an observation which these authors attribute to core polarization effects.

The isomeric states ($T_{\frac{1}{2}} > 5$ ns) have been identified in previous experiments [12-15]). Their excitation energies and γ-decay properties are well described by the shell-model calculations of Gloeckner and Serduke [16]) which assume a closed ^{88}Sr core with protons actively distributed in the $2p_{\frac{1}{2}}$ and $1g_{\frac{9}{2}}$ proton orbitals. Several new examples of significant shifts in the observed g-factors have been observed. The results demonstrate clearly that even the use of renormalized, "effective" g-factors in shell-model calculations may lead to quite inaccurate predictions.

The details of the measurements, their analysis and results are described in sect. 2. In sect. 3 the experimental g-factors are confronted with calculations of core polarization, evaluated in first-order perturbation theory. A calculation of contributions to the g-factors from one-pion exchange is presented in sect. 4.

2. Experimental procedures and results

2.1. THE EXPERIMENTS

Several heavy-ion induced reactions were employed to excite strongly and align the isomeric states of interest. The pulsed beam facility at the Chalk River MP

tandem produced sharp beam bursts of 2–5 ns duration and adjustable spacing (0.4–12.8 μs). The precession of the nuclear moment in an external magnet field was observed by measuring the time dependence of the intensity of deexcitation γ-rays, which were resolved in two Ge(Li) detectors placed at $\theta_\gamma = \pm 135°$. A detailed description of our methods used for time-differential measurements and of precautions taken to ensure high accuracy of the extracted g-factors is given elsewhere [17]).

Experimental difficulties arose for the long-lived isomers in ^{93}Tc ($T_{\frac{1}{2}} = 10$ μs) and ^{94}Ru ($T_{\frac{1}{2}} = 70$ μs), where previous experimenters [14,15]) observed the deexcitation γ-rays to exhibit isotropic angular distributions. The loss of alignment in these cases is most likely not caused by magnetic relaxation. The exponential decay of the nuclear alignment coefficient, $a_2(t) = a_2(0)\exp(-t/\tau_2)$ can be estimated for magnetic relaxation processes in metal hosts from the modified Korringa relation [18]) and a comprehensive compilation of chemical shifts [19]). We obtain spin lattice relaxation times, $\tau_2 \gtrsim 60$ μs, which are comparable to the longest half-lifes encountered. The most likely cause for the loss of alignment is therefore the interaction of the nuclear quadrupole moment with fluctuating electric field gradients in the solid [20]). We have chosen Pb and Hg as host materials because very long quadrupole relaxation times have been observed [cf. refs. [11,21])] for hosts at temperatures close to or above their melting points. The recoil energies associated with the conventional ^{4}He and ^{6}Li induced reactions [14]) are rather low ($\ll 3$ MeV), so that sufficient reaction yields would only be obtainable with multiple sandwiches of thin target-host layers. This difficulty was avoided by using ^{32}S and ^{35}Cl induced reactions, producing evaporation residues of large range (> 2 mg/cm^2). From a systematic study of various target-projectile combinations we established that the (^{35}Cl, 2p2n) and the (^{32}S,2p2n) reactions at $E = 120$–150 MeV had the highest production cross sections for the isomers of interest.

2.2. RESULTS

A summary of the experimental results is given in tables 1 and 2. The energies, identifications, and angular distribution coefficients $a_2(0)$ for the observed delayed γ-rays are shown in table 1. The energies quoted to a fraction of 1 keV have a typical error of 0.15 keV or less, otherwise they are accurate to the nearest keV. In table 2 properties of isomeric states are shown. The spin lattice relaxation times, τ_2, were obtained with host materials at room temperature (23 °C). The observed g-factors were corrected for diamagnetic shifts using the relativistic calculations of Feiock and Johnson [22]). A common Knight shift correction, $K = (0.75 \pm 0.25)\%$, was applied to all g-factors. The range of K is sufficiently broad to cover measured and calculated Knight shifts [19]) for metallic Sr, Nb, Mo and Tc, and in two cases, agrees with our determination of K deduced from the spin lattice relaxation times of table 2 (see discussion below).

In the following individual results are discussed in more detail.

TABLE 1

Angular distribution coefficients of delayed γ-rays

Nucleus	Reaction	E_γ [a] (keV)	J_i^π	J_f^π	Multi-polarity	$a_2\,(t=0)$ [b]
^{90}Zr	^{88}Sr(^{4}He, 2n)	141	8^+	6^+	E2	0.26 ± 0.02
		1129.14	6^+	5^-	E1	-0.24 ± 0.02
^{91}Nb	^{88}Sr(^{6}Li, 3n)	194	$\frac{13}{2}^-$	$\frac{9}{2}^-$	E2	0.24 ± 0.02
		1791	$\frac{9}{2}^-$	$\frac{9}{2}^+$	E1	0.29 ± 0.05
		1985	$\frac{13}{2}^-$	$\frac{9}{2}^+$	M2/E3	0.18 ± 0.04
^{92}Mo	^{65}Cu(^{32}S, 3p2n)	235	11^-	9^-	E2	0.22 ± 0.04
		626	9^-	7^-	E2	0.23 ± 0.03
	^{64}Ni(^{32}S, 2p2n)	1098	7^-	5^-	E2	0.23 ± 0.02
		244	5^-	4^+	E1	-0.17 ± 0.02
	^{90}Zr(^{4}He, 2n)	329.80	6^+	4^+	E2	0.28 ± 0.04
		772.97	4^+	2^+	E2	0.29 ± 0.03
		1509.68	2^+	0^+	E2	0.31 ± 0.03
^{93}Tc	^{65}Cu(^{32}S, 2p2n)	750.78	$\frac{17}{2}^-$	$\frac{13}{2}^+$	M2/E3	-0.20 ± 0.03 [b]
		629.44	$\frac{13}{2}^-$	$\frac{11}{2}^+$	E1	-0.15 ± 0.03
		711.11	$\frac{13}{2}^-$	$\frac{13}{2}^+$	E1	0.29 ± 0.03
		1434.52	$\frac{13}{2}^+$	$\frac{9}{2}^+$	E2	0.21 ± 0.03
		1515.8	$\frac{11}{2}^+$	$\frac{9}{2}^+$	M1/E2	-0.10 ± 0.03
^{94}Ru	^{92}Mo(^{4}He, 2n)	311.77	6^+	4^+	E2	0.23 ± 0.04
	^{63}Cu(^{35}Cl, 2p2n)	756.29	4^+	2^+	E2	0.25 ± 0.03
		1429.96	2^+	0^+	E2	0.27 ± 0.03

[a]) Error ±0.15 keV if fractions of keV are given.
[b]) The a_4 coefficients were generally small, except for the ^{93}Tc $\frac{17}{2}^- \rightarrow \frac{13}{2}^+$ transition ($a_4 = -0.25\pm0.05$).

TABLE 2

Properties of isomeric states

Nucleus	E_x (keV)	J	$T_{1/2}$	τ_2 (μs)	Host	g_{uncorr}	g [a]
^{90}Zr	3589	8^+	$134\ \pm4$ ns	$0.8\ \pm0.2$	Sr	$1.360\ \pm0.004$	1.356 ± 0.007
^{91}Nb	2035	$\frac{17}{2}^-$	3.4 ± 0.1 μs	0.90 ± 0.25	Sr	$1.277\ \pm0.013$	1.273 ± 0.016
^{92}Mo	4486	11^-	9.2 ± 0.5 ns		Hg	$1.266\ \pm0.022$	1.262 ± 0.025
	2760	8^+	$214\ \pm5$ ns	0.35 ± 0.04	Zr	$1.417\ \pm0.003$	1.413 ± 0.006
^{93}Tc	2185	$\frac{17}{2}^-$	10.1 ± 0.3 μs	80^{+50}_{-30}	Hg	$1.234\ \pm0.003$	1.231 ± 0.006
^{94}Ru	2643	8^+	$68\ \pm10$ μs	85^{+35}_{-20}	Hg	1.3913 ± 0.0012	1.387 ± 0.005
	2498	6^+	$65\ \pm2$ ns		Pb	1.3893 ± 0.0012	1.354 ± 0.008
					Mo	$1.357\ \pm0.004$	

[a]) Corrected for diamagnetic shift [22]) and Knight shift $K = (0.75\pm0.25)\%$.

The ^{90}Zr nucleus. The lowest 8^+ state at 3589 keV in ^{90}Zr was populated by the ^{88}Sr(^{4}He, 2n) reaction. Thick targets of natural Sr and pulsed 24 MeV ^{4}He beams with a pulse separation of 1.6 μs were used. The decay of the 8^+ isomer proceeds mainly through the long-lived 5^- state ($T_{\frac{1}{2}} \approx 800$ ms) and therefore only the 141 keV $8^+ \rightarrow 6^+$ E2 and the 1129.14 keV $6^+ \rightarrow 5^-$ E1 transitions were used for the

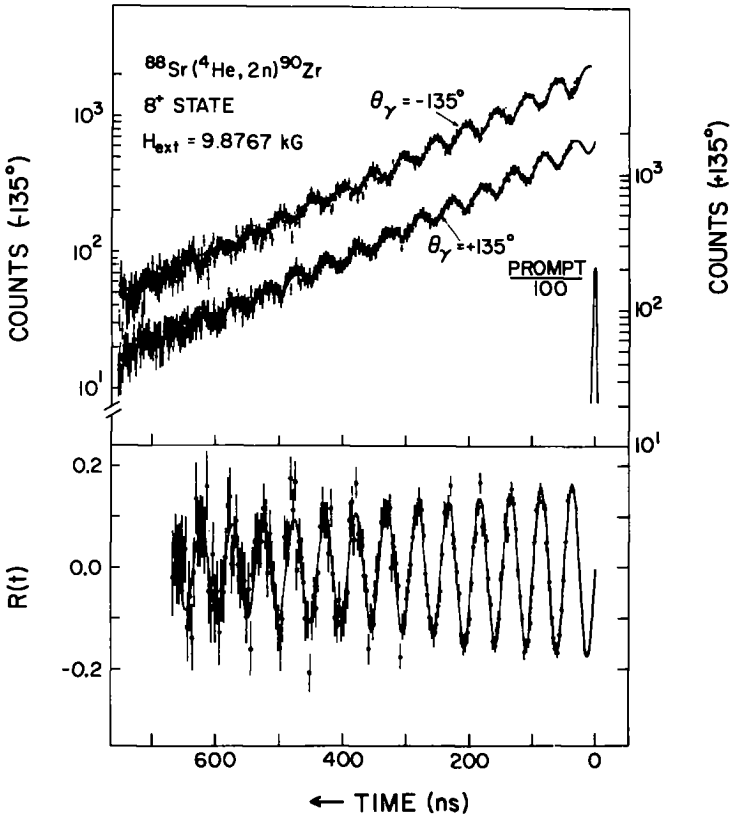

Fig. 1. Time distributions summed for the 141 keV E2 transition ($\theta_\gamma = \pm 135°$) and the 1139 keV E1 transition ($\theta_\gamma = \mp 135°$) in ^{90}Zr. The γ-angles refer to the 141 keV E2 transition. Also shown is the ratio of counting rates, $R(t) = (Y_1 - Y_2)/(Y_1 + Y_2)$.

analysis. To illustrate the results, time distributions showing oscillations of similar phase (i.e. for the 141 keV line at $\theta_\gamma = +135°$ and for the 1129.14 keV line at $\theta_\gamma = -135°$) were added and are shown in fig. 1. The four individual time distributions could be consistently fitted with $T_{\frac{1}{2}}(8^+) = 134 \pm 4$ ns, $\tau_2 = 800 \pm 200$ ns, and an uncorrected g-factor, $g_{\text{uncorr}}(8^+) = 1.360 \pm 0.004$. These measurements agree with but are more accurate than previous ones yielding [12,23]) $T_{\frac{1}{2}} = 125 \pm 6$ ns and $g_{\text{uncorr}}(8^+) = 1.367 \pm 0.015$.

The ^{91}Nb nucleus. The $\frac{17}{2}^-$ isomer [13]) at $E_x = 2035$ keV was populated by the ^{88}Sr(^{6}Li, 3n)^{91}Nb reaction by using pulsed 34 MeV ^{6}Li beams with a pulse separation of 12.8 μs. Again a thick target of natural Sr was employed. The 194 keV $\frac{13}{2}^- \rightarrow \frac{9}{2}^-$ E2, the 1985 keV $\frac{13}{2}^- \rightarrow \frac{9}{2}^+$ M2/E3, and the 1791 keV $\frac{9}{2}^- \rightarrow \frac{9}{2}^+$ E1 transitions have similarly large, positive a_2 angular distribution coefficients. The sum of their time distributions is shown in fig. 2. The data were best fitted with $T_{\frac{1}{2}}(\frac{17}{2}^-) = 3.4 \pm 0.1$ μs and $g_{\text{uncorr}}(\frac{17}{2}^-) = 1.277 \pm 0.013$. The observed relaxation time, $\tau_2 = 0.90 \pm 0.25$ μs,

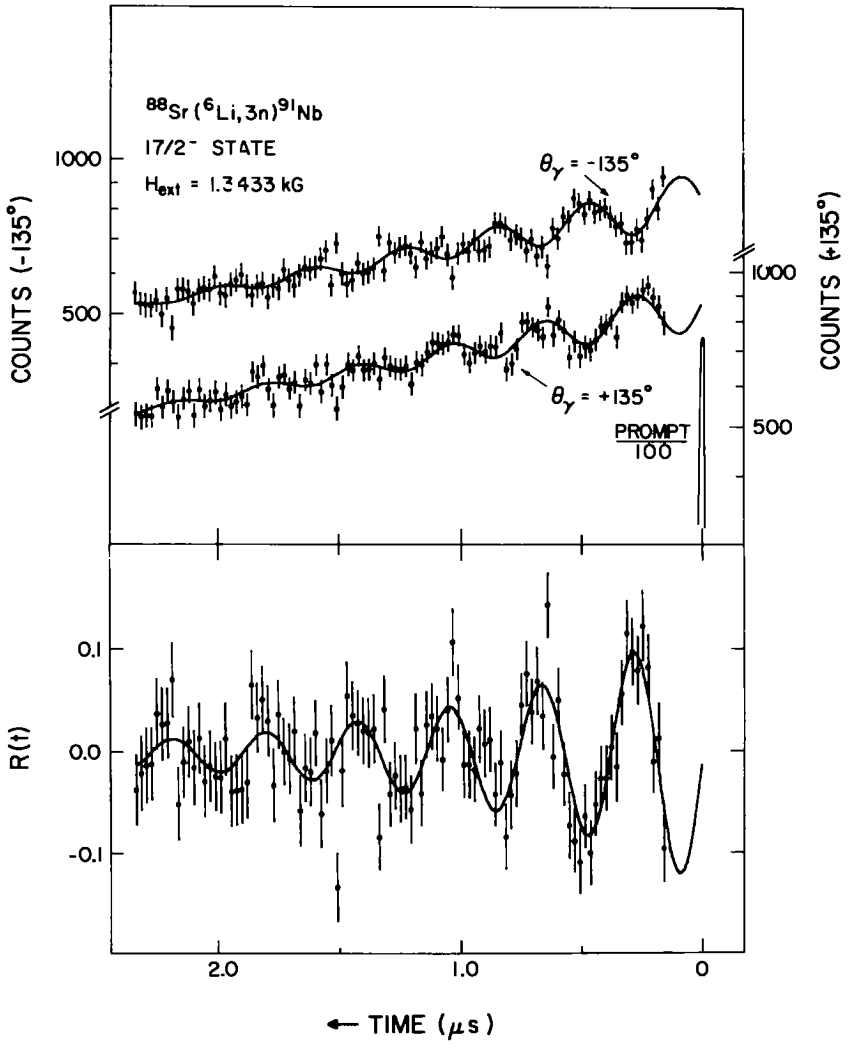

Fig. 2. Time distributions for the sum of the $\frac{13}{2}^- \rightarrow \frac{9}{2}^-$, $\frac{13}{2}^- \rightarrow \frac{9}{2}^+$ and $\frac{9}{2}^- \rightarrow \frac{9}{2}^+$ transitions in ^{91}Nb. The function $R(t)$ is also shown. Note that 1 kG = 0.1 T.

is much shorter than the half-life of the $\frac{17}{2}^-$ isomer and limits the accuracy with which the g-factor could be obtained. The previously measured value for this half-life [13]), $T_{\frac{1}{2}}(\frac{17}{2}^-) = 3.76 \pm 0.12$ μs is slightly longer than our best value.

From the measured a_2 coefficients the mixing ratio for the $\frac{13}{2}^- \rightarrow \frac{9}{2}^+$ transition has been calculated by using the $\frac{13}{2}^- \rightarrow \frac{9}{2}^-$ E2 transition to determine the alignment parameters of the isomeric state. Two solutions were obtained: for the 1985 keV transition: δ(E3/M2) = 0.11 ± 0.005 and $|\delta| > 15$; the sign convention is that of Rose and Brink [24]).

The ^{92}Mo nucleus. The 8^+ isomer at $E_x = 2760$ keV was populated by the ^{90}Zr(^{4}He, 2n)^{92}Mo reaction in thick targets of enriched ^{90}Zr. The bombarding energy, $E(^4\text{He}) = 24$ MeV was chosen to avoid substantial population of the 11^- isomer at 4486 keV. The beam pulse separation was 3.2 μs. The summed time distributions for the $6^+ \rightarrow 4^+$, $4^+ \rightarrow 2^+$ and $2^+ \rightarrow 0^+$ transitions are shown in fig. 3. From the individual time distributions we obtained $T_{\frac{1}{2}}(8^+) = 214 \pm 5$ ns and $g_{\text{uncorr}}(8^+) = 1.417 \pm 0.003$. The half-life is somewhat longer than the value 191 ± 7 ns obtained by Cochavi *et al.* [25]). The g-factor agrees with the result of Nagamiya *et al.* [12]), $g_{\text{uncorr}}(8^+) = 1.421 \pm 0.013$, but is more precise.

The 11^- isomer at $E_x = 4486$ keV was strongly populated by the ^{65}Cu(^{32}S, 3p2n)^{92}Mo and by the ^{64}Ni(^{32}S, 2p2n)^{92}Mo reactions at $E(^{32}\text{S}) = 132$ MeV. The targets consisted of 1.6 mg/cm^2 thick foils backed by liquid mercury. A large fraction

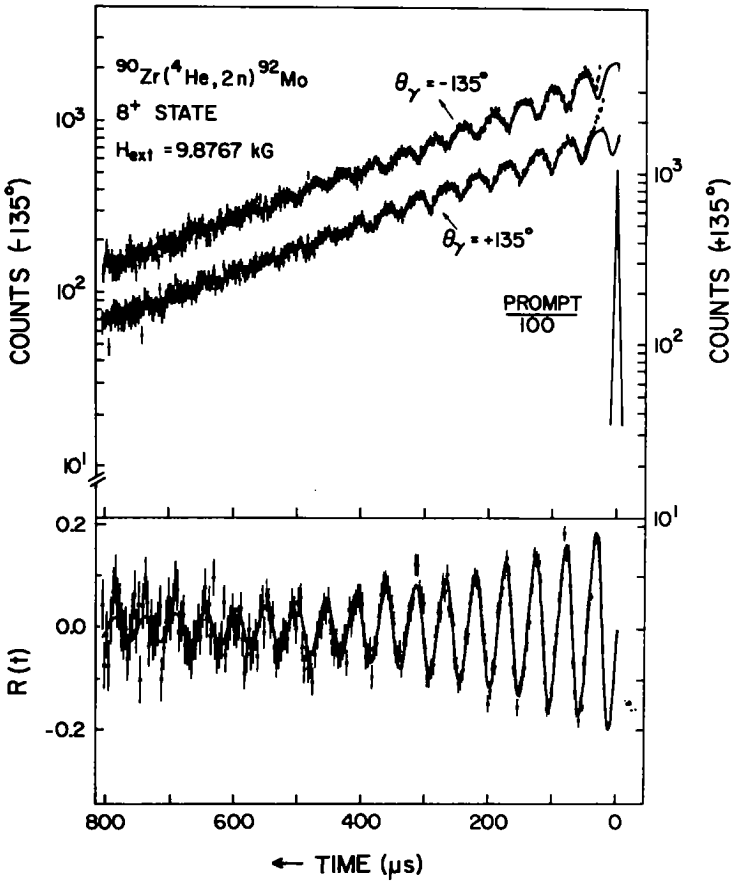

Fig. 3. Time distributions for the sum of the $6^+ \rightarrow 4^+$, $4^+ \rightarrow 2^+$ and $2^+ \rightarrow 0^+$ transitions in ^{92}Mo. The fits shown include spin-lattice relaxation effects as described in the text. Note that 1 kG = 0.1 T.

of the yrast cascade passes apparently through the 11^- state and almost completely avoids population of the lower-lying 8^+ state. The time distributions, appropriately summed for γ-rays in the cascade $11^- \rightarrow 9^- \rightarrow 7^- \rightarrow 5^- \rightarrow 4^+ \rightarrow 2^+ \rightarrow 0^+$ are shown in fig. 4. The constant background at times $T > 10$ ns arises from radioactive decay of 4.4 min ^{92}Tc which populates strongly the 2760 keV 8^+ state in ^{92}Mo. From a fit to the individual time distributions we obtained a half-life, $T_{\frac{1}{2}}(11^-) = 9.2 \pm 0.5$ ns and an uncorrected g-factor, $g_{\text{uncorr}}(11^-) = 1.266 \pm 0.022$. The half-life is in good agreement with the value $T_{\frac{1}{2}}(11^-) = 8.8 \pm 0.5$ ns, as determined by Jaklevic, Lederer and Hollander [14]).

The ^{93}Tc nucleus. The $\frac{17}{2}^-$ isomer at $E_x = 2185$ keV was populated strongly by the ^{65}Cu(^{32}S, 2p2n)^{93}Tc reaction at $E(^{32}\text{S}) = 120$ MeV. The evaporation residues recoiled out of the 1.5 mg/cm^2 thick ^{65}Cu foil into a liquid mercury backing. The effectiveness of the Hg host in maintaining the initial alignment of the isomeric state was tested with 0.5 μs wide beam pulses spaced by 100 μs and weak magnetic fields of 5 mT. For this rather long time scale, we employed a beam pulse controller and a digital timer unit built at CRNL [26]). Time distributions were obtained for all γ-rays

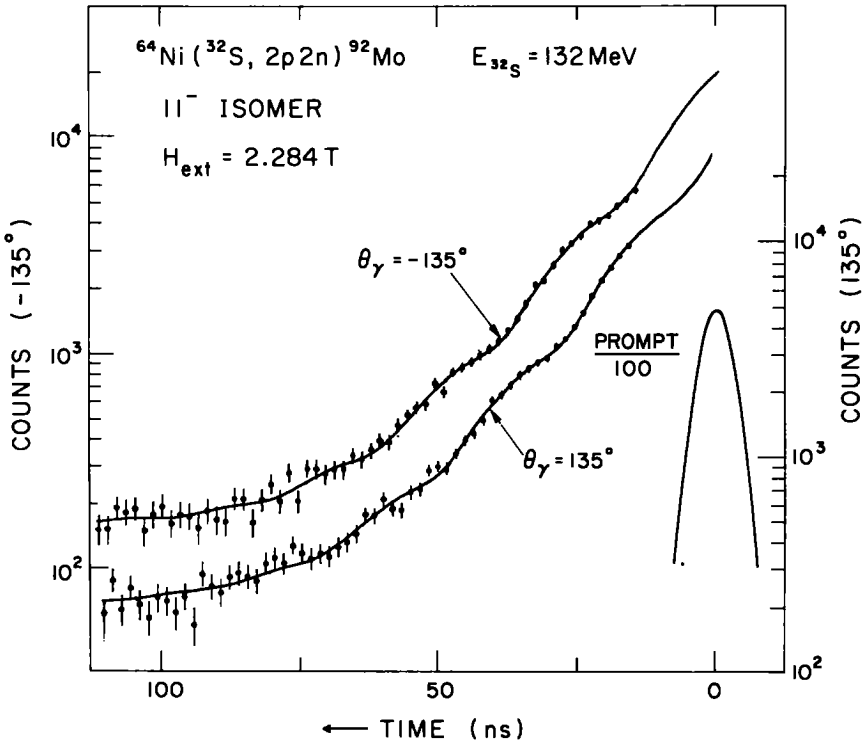

Fig. 4. Time distributions for the sum of E2 transitions in the γ-cascade de-exciting the 11^- isomer in ^{92}Mo. The constant background at large times arises from the decay of 4.4 min ^{92}Tc produced by the bombardment of ^{65}Cu with 132 MeV ^{32}S.

except for the low-energy (40 keV) $\frac{17}{2}^- \rightarrow \frac{13}{2}^-$ E2 transition. From these time distributions we obtained the a_2 coefficients quoted in table 1. They are in agreement with a recent very accurate angular distribution measurement [27]) using the same reaction. The extraction of mixing ratios and the significance of the angular distribution for the 750.78 keV $\frac{17}{2}^- \rightarrow \frac{13}{2}^+$ transition to a possible parity-violating admixture in the $\frac{17}{2}^-$ state is discussed elsewhere [27]). The half-life from the present work, $T_{\frac{1}{2}}(\frac{17}{2}^-) = 10.1 \pm 0.3$ μs, is in good agreement with the value 10.5 ± 0.7 μs measured by Brown *et al.* [15]). The observed relaxation time, $\tau_2 = 80^{+50}_{-30}$ μs, is much longer and could only be approximately determined. Assuming quadrupole relaxation for Tc($\frac{17}{2}^-$) in Hg to be negligible, the relaxation time corresponds [18]) to a Knight shift, $K(\mathrm{Tc}Hg) = (1.0 \pm 0.3)\%$. This value is comparable to Knight shifts for this mass region [19]) and thus supports the assumption that quadrupole interactions in Hg no longer provide the dominant mechanism for spin-lattice relaxation.

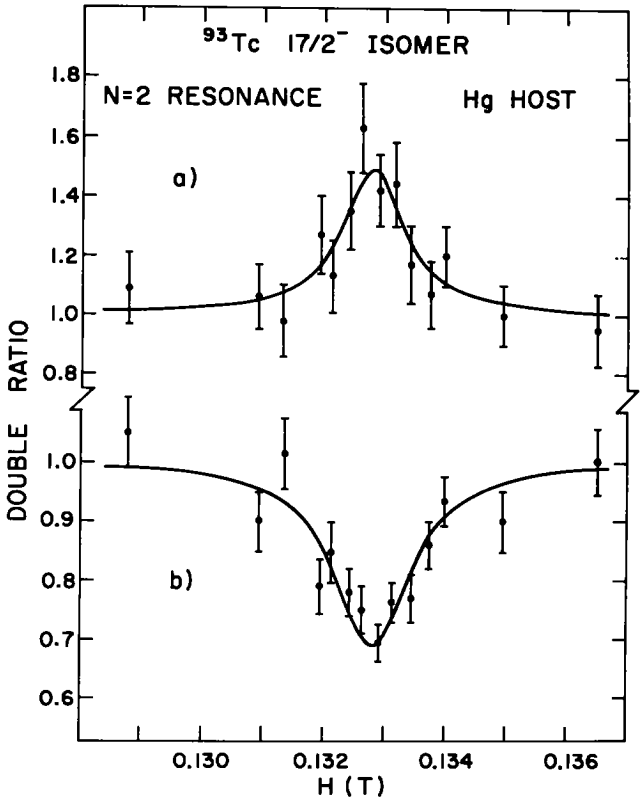

Fig. 5. Stroboscopic $n = 2$ resonance for five γ-rays de-exciting the $\frac{17}{2}^-$ isomer in ^{93}Tc. Two of these exhibit a positive a_2 (upper half, (a)), the others a negative a_2 (lower half, (b)). The time interval between beam pulses was 800 ns and the two γ-detectors were located at $\pm 135°$ to the beam axis. The double ratio of counting rates is defined in ref. [28]). The fitted curve represents an exact numerical calculation of R.

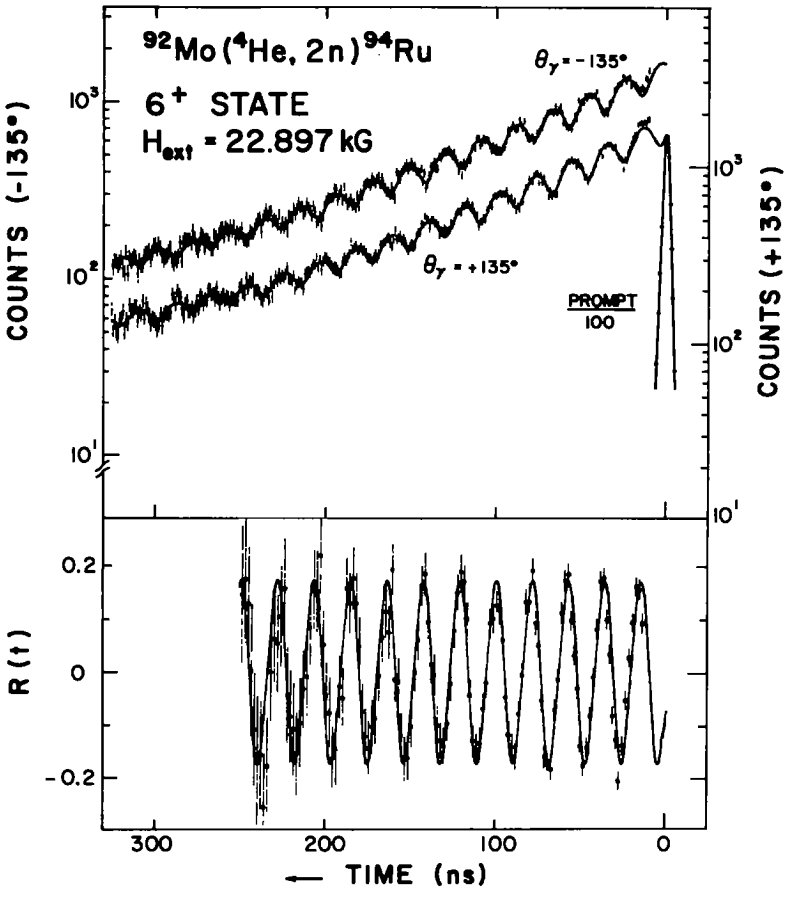

Fig. 6. Time distribution for the sum of three E2 γ-rays de-exciting the 6^+ isomer in ^{94}Ru. Data points for the first 30 ns after the prompt beam burst were excluded from the fit.

The magnetic moment of the $\frac{17}{2}^-$ isomer was measured accurately under the same bombarding conditions. The pulsed beam stroboscopic technique [28]) was used to obtain the data shown in fig. 5. At pulse repetition times of 800 ns the $n = 2$ resonance was observed at 0.1329 ± 0.0003 T, corresponding to an uncorrected g-factor, $g_{\text{uncorr}}(\frac{17}{2}^-) = 1.234 \pm 0.003$.

The ^{94}Ru nucleus. The 6^+ isomer at $E_x = 2498$ keV was populated by the ^{92}Mo(^{4}He, 2n)^{94}Ru reaction. At $E(^4\text{He}) = 25$ MeV the higher lying 8^+ isomer which has a much longer half-life [14]) and decays to the 6^+ state, was only weakly populated. The time distributions for the combined 311.77 keV $6^+ \rightarrow 4^+$, 756.29 keV $4^+ \rightarrow 2^+$, and the 1429.96 keV $2^+ \rightarrow 0^+$ transitions are shown in fig. 6. The first 30 ns after the prompt beam pulse were excluded from the fit because of a short half-life component in the decay of the 4^+ state. The fitted half-life, $T_{\frac{1}{2}}(6^+) = 65 \pm 2$ ns

agrees with a previous measurement [14]) yielding the value 74 ± 7 ns. An uncorrected g-factor, $g_{\text{uncorr}}(6^+) = 1.357 \pm 0.004$, was also obtained.

The long-lived 8^+ isomer at $E_x = 2643$ keV was strongly populated by the ^{63}Cu(^{35}Cl, 2p2n)^{94}Ru reaction at $E(^{35}\text{Cl}) = 120$ MeV. Angular distribution coefficients, half-life, relaxation times and approximate g-factors were obtained for this isomer with a Hg backed ^{65}Cu target. The slow beam pulsing system [26]) and a weak external magnetic field (1.6 mT) were used. The beam pulses were 0.5 μs wide separated by 500 μs. The time distributions showed slight deviations from an exponential decay with a single half-life. These distortions are likely caused by pileup effects resulting from the high probability of detecting a prompt γ-ray per beam pulse. The accuracy for the extracted half-life $T_{\frac{1}{2}}(8^+) = 68 \pm 10$ μs, and of the relaxation time, $\tau_2 = 85^{+35}_{-20}$ μs, was rather poor. The half-life agrees with a previous measurement [14]), yielding $T_{\frac{1}{2}}(8^+) = 71 \pm 5$ μs. The observed relaxation time corresponds [18]) to a Knight shift, $K(\text{Ru}Pb) = (0.86 \pm 0.14)\%$, neglecting again quadrupole interactions.

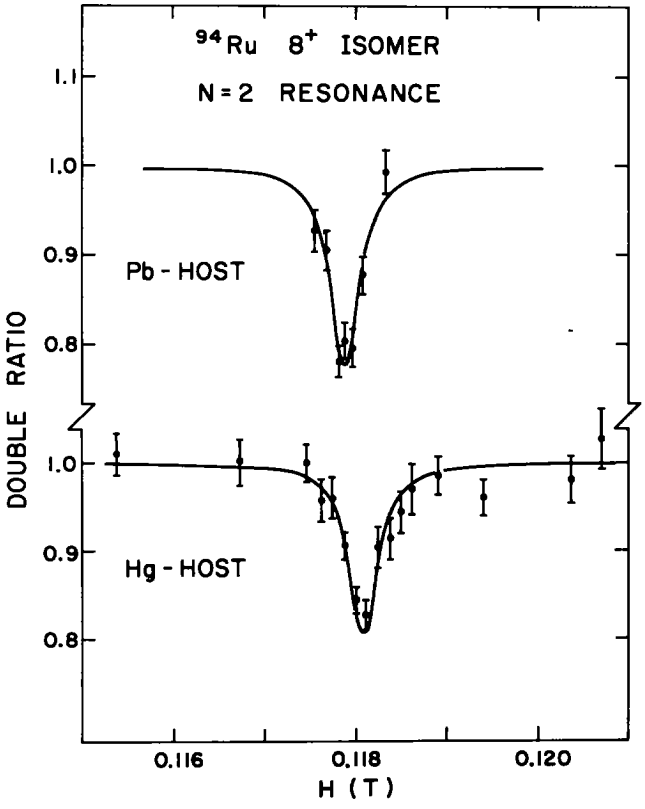

Fig. 7. Stroboscopic $n = 2$ resonances for the sum of three E2 transitions de-exciting the 8^+ isomer in ^{94}Ru. The resonances are slightly shifted for the two hosts. See also caption for fig. 5.

A precise measurement of the magnetic moment of the 8^+ state was made with both Hg and Pb backed ^{63}Cu targets. The data in fig. 7 were obtained by the pulsed beam stroboscopic technique [28]). At a pulsed beam repetition time of 800 ns the $n = 2$ resonances were observed at 0.11786 ± 0.00010 T and 0.11803 ± 0.00010 T for hosts of Hg and Pb, respectively. The small shift in the resonance field of $(0.14 \pm 0.17)\%$ is interpreted as a nearly insignificant difference in the chemical shifts, $K(\mathrm{Ru}Hg)$ and $K(\mathrm{Ru}Pb)$. Since the Knight shifts [19]) for the host materials, $K(\mathrm{Hg}Hg) = 2.7\%$ and $K(\mathrm{Pb}Pb) = 1.5\%$, are very different, our result demonstrates that chemical shifts are frequently rather independent of the host material.

3. Discussion of g-factors

The isomeric states whose g-factors have been measured in the present study (see table 2) have as a common feature a closed $N = 50$ neutron shell. The shell-model calculations of Gloeckner and Serduke [16]) describe successfully the energy spectra in these nuclei through the construction of an effective interaction for valence protons in the $2p_{\frac{1}{2}}$ and $1g_{\frac{9}{2}}$ orbitals. The observed $B(\mathrm{E2})$ and $B(\mathrm{M1})$ values are likewise well explained, provided an effective charge parameter and effective g-factors are introduced.

For the M1 operator, it is a long established result of angular momentum algebra [29]) that for mixed configurations in two valence orbitals, j_1 and j_2, the g-factors can be written

$$g(J) = \langle j_1^{n_1} J_1, j_2^{n_2} J_2; J \| T^{(1)} \| j_1^{n_1} J_1 j_2^{n_2} J_2; J \rangle / [J(J+1)]^{\frac{1}{2}}$$

$$= \tfrac{1}{2}(g_1 + g_2) + \frac{J_1(J_1+1) - J_2(J_2+1)}{2J(J+1)}(g_1 - g_2), \qquad (1)$$

where $g_i = \langle j_i \| T^{(1)} \| j_i \rangle / [j_i(j_i+1)]^{\frac{1}{2}}$ is the g-factor for orbital i, and $T^{(1)}$ is a one-body spherical tensor of rank one. Clearly the g-factor of state J is independent of the orbit occupancy, n_1 and n_2. This statement is often referred to as the additivity rule and implies (see below) that the g-factors of 8^+ and 6^+ states in ^{90}Zr, ^{92}Mo and ^{94}Ru should be the same, and the $\frac{17}{2}^-$ states in ^{91}Nb and ^{93}Tc should likewise be constant. The results of table 2 show a small but significant breakdown of the additivity rule (see also fig. 8). It will be shown that this breakdown can be understood as a core polarization correction.

For the nuclei in question, we adopt, to a zeroth-order approximation, amplitudes for the configuration mixing between the $2p_{\frac{1}{2}}$ and $1g_{\frac{9}{2}}$ orbitals from Gloeckner and Serduke:

$$|^{90}\mathrm{Zr}, 8^+\rangle = |p_{\frac{1}{2}}^0(0), g_{\frac{9}{2}}^2(8); 8\rangle,$$

$$|^{91}\mathrm{Nb}, \tfrac{17}{2}^-\rangle = |p_{\frac{1}{2}}^1(\tfrac{1}{2}), g_{\frac{9}{2}}^2(8); \tfrac{17}{2}\rangle,$$

$$|^{92}\mathrm{Mo}, 11^-\rangle = |p_{\frac{1}{2}}^1(\tfrac{1}{2}), g_{\frac{9}{2}}^3(\tfrac{21}{2}); 11\rangle,$$

$$
\begin{aligned}
|^{92}\mathrm{Mo}, 8^+\rangle &= 0.888|\mathrm{p}_{\frac{1}{2}}^2(0), \mathrm{g}_{\frac{9}{2}}^2(8); 8\rangle - 0.460|\mathrm{p}_{\frac{1}{2}}^0(0), \mathrm{g}_{\frac{9}{2}}^4(8); 8\rangle,\\
|^{93}\mathrm{Tc}, \tfrac{17}{2}^-\rangle &= |\mathrm{p}_{\frac{1}{2}}^1(\tfrac{1}{2}), \mathrm{g}_{\frac{9}{2}}^4(8); \tfrac{17}{2}\rangle,\\
|^{94}\mathrm{Ru}, 8^+\rangle &= 0.905|\mathrm{p}_{\frac{1}{2}}^2(0), \mathrm{g}_{\frac{9}{2}}^4(8); 8\rangle - 0.425|\mathrm{p}_{\frac{1}{2}}^0(0)\mathrm{g}_{\frac{9}{2}}^6(8); 8\rangle,\\
|^{94}\mathrm{Ru}, 6^+\rangle &= 0.905|\mathrm{p}_{\frac{1}{2}}^2(0), \mathrm{g}_{\frac{9}{2}}^4(6); 6\rangle - 0.425|\mathrm{p}_{\frac{1}{2}}^0(0)\mathrm{g}_{\frac{9}{2}}^6(6); 6\rangle. \qquad (2)
\end{aligned}
$$

Application of eq. (1) to these configurations leads to the expectation that

$$
\begin{gathered}
g(^{90}\mathrm{Zr}, 8^+) = g(^{92}\mathrm{Mo}, 8^+) = g(^{94}\mathrm{Ru}, 8^+) = g_2,\\
g(^{91}\mathrm{Nb}, \tfrac{17}{2}^-) = g(^{93}\mathrm{Tc}, \tfrac{17}{2}^-) = \tfrac{1}{17}g_1 + \tfrac{16}{17}g_2,\\
g(^{92}\mathrm{Mo}, 11^-) = \tfrac{1}{22}g_1 + \tfrac{21}{22}g_2,
\end{gathered}
$$

where g_1 is the single-particle g-factor in the $\mathrm{p}_{\frac{1}{2}}$ orbital [g(Schmidt) = -0.526] and g_2 that for the $g_{\frac{9}{2}}$ orbit [g(Schmidt) = 1.510]. Examination of the experimental data in fig. 8 shows a breakdown of these simple expectations by approximately 5 %.

First-order core polarization corrections to g-factors arise only from particle-hole excitations in which the single particle with spin $j = l \pm \frac{1}{2}$ interacts with its spin-orbit partner $j = l \mp \frac{1}{2}$. For a ^{88}Sr core and an active configuration space of $\pi(\mathrm{p}_{\frac{1}{2}}^{n_1}\mathrm{g}_{\frac{9}{2}}^{n_2})$ there are only three such core excitations corresponding to two proton $\pi(\mathrm{p}_{\frac{1}{2}}^{-1}\mathrm{p}_{\frac{1}{2}}^{n_1+1}\mathrm{g}_{\frac{9}{2}}^{n_2})$ and $\pi(\mathrm{p}_{\frac{1}{2}}^{n_1}\mathrm{g}_{\frac{9}{2}}^{n_2-1}\mathrm{g}_{\frac{7}{2}})$ and one neutron $\pi(\mathrm{p}_{\frac{1}{2}}^{n_1}\mathrm{g}_{\frac{9}{2}}^{n_2})\nu(\mathrm{g}_{\frac{9}{2}}^{-1}\mathrm{g}_{\frac{7}{2}})$ excitations. The relevant first-order core polarization diagrams are drawn in fig. 9 (all time orderings implied).

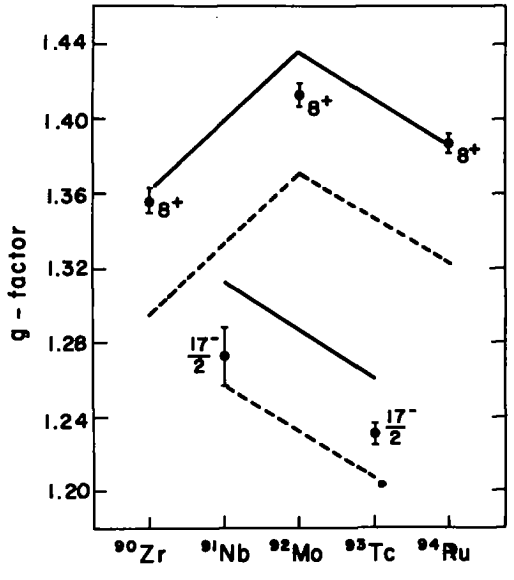

Fig. 8. Experimental g-factors for the 8^+ and $\frac{17}{2}^-$ isomers in $N = 50$ nuclei. The solid lines are theoretical calculations from table 3 (including both core polarization and meson exchange current corrections). The dashed line only includes the core polarization correction.

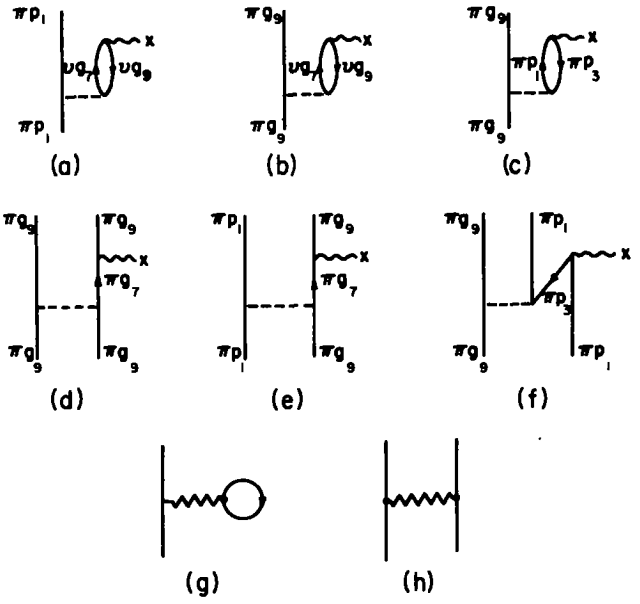

Fig. 9. Goldstone diagrams detailing the first-order core polarization and meson exchange current corrections to magnetic moments. Diagrams (a), (b), (c) and (g) are one-body graphs; (d), (e), (f) and (h) two-body graphs. Only two-body graphs contribute to the breakdown in the additivity rule. In graphs (g) and (h), the jagged line represents the two-body meson-exchange operator, eq. (4), as detailed in fig. 10.

Notice there are three one-body diagrams (a)–(c), and three two-body diagrams, (d)–(f). This is a familiar situation arising in the theory of effective operators [30]. The truncation from an infinite dimensional Hilbert space to a small, finite, model space, in this case $\pi(p_{\frac{1}{2}}^{n_1}, g_{\frac{7}{2}}^{n_2})$, and the requirement that the transition matrix element of an effective operator in the model space should be the same as the true, one-body operator in the infinite space leads to an effective operator of many-body character. In first-order perturbation theory, the effective operator has one-body and two-body terms.

For the many-particle configurations listed in eq. (2), the evaluation of the effective one-body part of the operator is still given by eq. (1), with g_1 now interpreted as the Schmidt value for a $p_{\frac{1}{2}}$ proton plus the contribution from diagram (a), while g_2 is the Schmidt value for a $g_{\frac{7}{2}}$ proton plus the contribution from diagrams (b) and (c). For the two-body part of the operator, the matrix element is given by

$$\langle j_1^{n_1} J_1, j_2^{n_2} J_2; J \| T^\lambda \| j_1^{n_1} J_1, j_2^{n_2} J_2; J \rangle$$

$$= \tfrac{1}{2} n_1 (n_1 - 1) U(J J_2 \lambda J_1, J_1 J) \sum_{\sigma \mu \mu'} \langle j_1^{n_1} J_1 \{ | j_1^{n_1 - 2} \sigma; j_1^2 \mu \rangle$$

$$\times \langle j_1^{n_1} J_1 \{ | j_1^{n_1 - 2} \sigma; j_1^2 \mu' \rangle U(\mu' \lambda \sigma J_1; \mu J_1) \langle j_1^2; \mu \| T^\lambda \| j_1^2; \mu' \rangle$$

$$+\tfrac{1}{2}n_2(n_2-1)U(JJ_1\lambda J_2;J_2J)\sum_{\sigma\mu\mu'}\langle j_2^{n_2}J_2\{|j_2^{n_2-2}\sigma;j_2^2\mu\rangle$$

$$\times\langle j_2^{n_2}J_2\{|j_2^{n_2-2}\sigma;j_2^2\mu'\rangle U(\mu'\lambda\sigma J_2;\mu J_2)\langle j_2^2;\mu\|T^\lambda\|j_2^2;\mu'\rangle$$

$$+n_1n_2\sum_{\substack{\sigma_1\sigma_2\\ \mu\mu'}}\langle j_1^{n_1}J_1\{|j_1^{n_1-1}\sigma_1\rangle^2\langle j_2^{n_2}J_2\{|j_2^{n_2-1}\sigma_2\rangle^2\begin{bmatrix}\sigma_1 & j_1 & J_1\\ \sigma_2 & j_2 & J_2\\ \phi & \mu & J\end{bmatrix}$$

$$\times\begin{bmatrix}\sigma_1 & j_1 & J_1\\ \sigma_2 & j_2 & J_2\\ \phi & \mu' & J\end{bmatrix}U(\mu'\lambda\phi J;\mu J)\langle j_1j_2;\mu\|T^\lambda\|j_1j_2;\mu'\rangle, \qquad (3)$$

where the two-body matrix elements on the right-hand side are the contributions from diagrams (d)–(f) evaluated between normalized, antisymmetrized two-particle states. Here $\langle\ldots\{|\ldots\rangle$ are fractional parentage coefficients [29]), $U(\ldots)$ are Jahn's recoupling coefficients, and [ ] are normalized $9j$ coefficients.

To evaluate the diagrams in fig. 9, the standard M1 operator with free nucleon coupling constants was used at the single-particle vertices and a central particle-hole force [Yukawa shape, strength -50 MeV, range 1.54 fm and exchange force mixture as given by Perez [31]) for particle-hole states in ^{16}O and ^{40}Ca] was used for the two-particle vertices. All radial integrals were evaluated with harmonic oscillator wave functions, $\hbar\omega = 9.22$ MeV. Energy denominators were taken from the binding energies of the closed shell (plus or minus one) nuclei, and were for the $p_{\frac{3}{2}}$-$p_{\frac{1}{2}}$ splitting 3.537 MeV and for the $g_{\frac{9}{2}}$-$g_{\frac{7}{2}}$ splitting 7.423 MeV.

TABLE

Contribution from each diagram in fig. 9 to

Config.	$p^0g^2(8)$	$p^1g^2(8);\frac{1}{2}^7$	$p^2g^2(8)$	$p^0g^4(8)$	$p^1g^4(8);\frac{1}{2}^7$
Schmidt	1.510	1.390	1.510	1.510	1.390
a		0.011			0.011
b	−0.089	−0.084	−0.089	−0.089	−0.084
c	−0.109	−0.103	−0.109	−0.109	−0.103
d	−0.016	−0.015	−0.016	−0.070	−0.066
e		0.001			0.004
f		0.057	0.109		0.053
g	0.067	0.057	0.067	0.067	0.057
h	−0.001	−0.001	−0.001	−0.003	−0.003
sum	1.361	1.313	1.471	1.306	1.261
				1.436 [a])	
g_{exp} [b])	1.356	1.273		1.413	1.231
	±0.007	±0.016		±0.006	±0.006

[a]) Weighted average according to the configuration mixing amplitudes of
[b]) From table 2.

The contribution to the g-factor from each diagram in fig. 9 is itemized in table 3 for each of the many-particle configurations listed in eq. (2). Notice that when the $p_{\frac{1}{2}}$ shell is completely filled, the contribution from diagram (c) is exactly cancelled by that from diagram (f). This is a general result [5]) indicating that when a subshell such as the $p_{\frac{1}{2}}$ is closed, the core polarization correction from the particle-hole excitation, e.g. $(p_{\frac{1}{2}}^{-1}p_{\frac{1}{2}})$, vanishes. This is reflected in the experimental data where the g-factor for ^{92}Mo(8^+) shows the smallest deviation from the Schmidt value ($g = 1.510$).

The decrease in the g-factors from ^{91}Nb$(\frac{17}{2}^-)$ to ^{93}Tc$(\frac{17}{2}^-)$ and from ^{92}Mo(8^+) to ^{94}Ru(8^+) is a result of the buildup of the $\pi g_{\frac{9}{2}}^{n_2-1}g_{\frac{7}{2}}$ core polarization arising from diagram (d). The small g-factor for ^{90}Zr(8^+) results from the sizeable first-order $\pi(p_{\frac{1}{2}}^{-1}p_{\frac{1}{2}})$ correction, which is large because the energy denominator associated with this excitation is small.

The only qualitative discrepancy between the present approach and observation concerns the difference of g-factors, $\Delta = g(^{94}\text{Ru}, 8^+) - g(^{94}\text{Ru}, 6^+) = 0.033 \pm 0.013$, whereas our calculation suggests $\Delta \approx 0$. Two effects can be found which tend to reduce the g-factor of the 6^+ state. Firstly, it has been noticed by Gloeckner and Serduke [16]) that the small $B(\text{E2}, 8^+ \rightarrow 6^+)$ cannot be explained by a seniority conserving interaction. Using their seniority breaking interaction [16]) obtained from fitting several B(E2) values, we calculate $\Delta \approx 0.007$. Secondly, one may have core excited proton configurations of

$$\{[2p_{\frac{1}{2}}^{-2}1f_{\frac{7}{2}}^{-2}]J, p_{\frac{1}{2}}^2 g_{\frac{9}{2}}^8 0; J\} \quad \text{and} \quad \{[p_{\frac{1}{2}}^{-1}f_{\frac{7}{2}}^{-2}p_{\frac{1}{2}}]J, g_{\frac{9}{2}}^6 0; J\}$$

that can contribute to the $J = 6$, but not to the $J = 8$ state. We estimate that an admixture of about 4% is required to account for the remaining discrepancy in Δ.

3

the g-factors of high spin isomers in $N = 50$ nuclei

$p^2g^4(8)$	$p^0g^6(8)$	$p^2g^4(6)$	$p^0g^6(6)$	$p^1g^3(\frac{21}{2})$; 11	$p_{3/2}^{-1}$	$p_{1/2}$
1.510	1.510	1.510	1.510	1.417	2.529	−0.529
				0.009	−0.333	0.192
−0.089	−0.089	−0.089	−0.089	−0.085		
−0.109	−0.109	−0.109	−0.109	−0.104	−0.707	
−0.070	−0.123	−0.074	−0.119	−0.035		
				0.002		
0.109		0.109		0.056		
0.067	0.067	0.067	0.067	0.059	0.108	−0.110
−0.003	−0.005	−0.003	−0.005	−0.002		
1.416	1.250	1.411	1.254	1.316	1.597	−0.446
1.386 [a])		1.382 [a])				
1.387		1.354		1.262	1.8344	−0.2747
±0.005		±0.008		±0.025		

Gloeckner and Serduke [16]).

4. Meson exchange current correction

We now turn our attention to the second major correction to magnetic moments, namely, that arising from meson exchange currents. Our results are listed in rows (g) and (h) in table 3. The calculation follows precisely the method given by Chemtob and Rho [3]) and reference can be made to that paper for further details. Only the one-pion exchange process has been considered.

The two-body magnetic moment exchange operator has an isovector and isoscalar component of general form:

$$H^{v} = \tfrac{1}{2}\{(\tau(1)\times\tau(2))[(\sigma_1\times\sigma_2)g_{\mathrm{I}}+T_{12}^{(\times)}g_{\mathrm{II}}]+[\tau(1)-\tau(2)][(\sigma_1-\sigma_2)h_{\mathrm{I}}+T_{12}^{(-)}h_{\mathrm{II}}]$$
$$+[\tau(1)+\tau(2)][(\sigma_1+\sigma_2)j_{\mathrm{I}}+T_{12}^{(+)}j_{\mathrm{II}}]+(\tau(1)\times\tau(2))(\hat{r}\times\hat{R})[(\sigma_1\cdot\sigma_2)n_{\mathrm{I}}+S_{12}n_{\mathrm{II}}]\},$$
$$H^{s} = \tfrac{1}{2}\{[\tau(1)\cdot\tau(2)][(\sigma_1+\sigma_2)m_{\mathrm{I}}+T_{12}^{(+)}m_{\mathrm{II}}]\}, \qquad (4)$$

where only terms contributing to the one-pion exchange process have been retained in eq. (4). In the above expression g_{I}, g_{II}, h_{I}, etc. are real scalar functions of $|r| = r$, and S_{12} and T_{12} signify the following operators:

$$S_{12} = 3(\sigma_1\cdot\hat{r})(\sigma_2\cdot\hat{r})-(\sigma_1\cdot\sigma_2),$$

$$T_{12} = [(\sigma_1\odot\sigma_2)\cdot\hat{r}\hat{r}-\tfrac{1}{3}(\sigma_1\odot\sigma_2)], \qquad \odot = \pm, \times,$$

where $r = \hat{r}/|r|$. The explicit forms of the radial functions are set out in the following subsections.

4.1. PIONIC CURRENT AND PAIR EXCITATION CURRENT (Figs. 10a–c)

$$g_{\mathrm{I}} = -\frac{2}{3}\frac{M}{m_\pi}f_{\pi\mathrm{NN}}^2(1-2x)Y_0(x), \qquad g_{\mathrm{II}} = -2\frac{M}{m_\pi}f_{\pi\mathrm{NN}}^2(1+x)Y_0(x),$$

$$n_{\mathrm{I}} = \frac{2}{3}\frac{M}{m_\pi}f_{\pi\mathrm{NN}}^2|r||R|Y_0(x), \qquad n_{\mathrm{II}} = \frac{2}{3}\frac{M}{m_\pi}f_{\pi\mathrm{NN}}^2|r||R|Y_2(x),$$

where $x = m_\pi r$, with m_π the pion mass, M the nucleon mass and $f_{\pi\mathrm{NN}}$ the pion-nucleon coupling constant ($f_{\pi\mathrm{NN}}^2 = 0.08$). The radial functions are

$$Y_0(x) = \frac{\mathrm{e}^{-x}}{x}, \qquad Y_2(x) = \left(1+\frac{3}{x}+\frac{3}{x^2}\right)Y_0(x).$$

4.2. NUCLEON ISOBARS (Figs. 10d, e)

$$g_{\mathrm{I}} = \tfrac{2}{9}(\gamma_{\mathrm{p}}-\gamma_{\mathrm{n}})h_1(0)m_\pi^3Y_0(x), \qquad g_{\mathrm{II}} = -\tfrac{1}{3}(\gamma_{\mathrm{p}}-\gamma_{\mathrm{n}})h_1(0)m_\pi^3Y_2(x),$$

$$h_{\mathrm{I}} = j_{\mathrm{I}} = -\tfrac{2}{9}(\gamma_{\mathrm{p}}-\gamma_{\mathrm{n}})h_2(0)m_\pi^3Y_0(x), \qquad h_{\mathrm{II}} = j_{\mathrm{II}} = -\tfrac{2}{3}(\gamma_{\mathrm{p}}-\gamma_{\mathrm{n}})h_2(0)m_\pi^3Y_2(x),$$

where h_1 and h_2 are combinations of p-wave scattering amplitudes: $h_1(0)m_\pi^3 = 0.074$

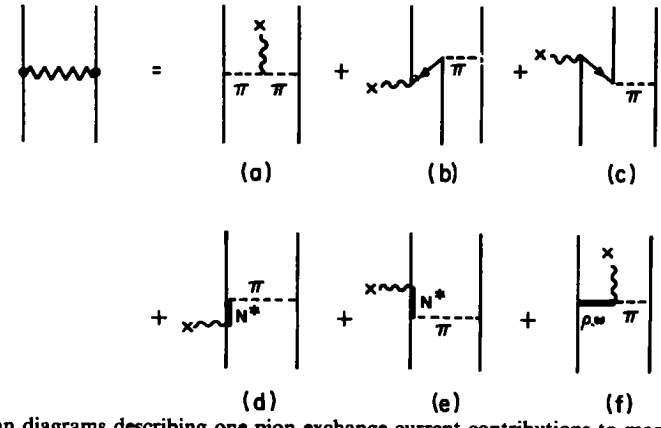

Fig. 10. Feynman diagrams describing one-pion exchange current contributions to magnetic moments. The jagged line on the left symbolises the sum of the six diagrams on the right. Graph (a) displays the contribution from pionic currents, (b) and (c) pair-excitation currents, (d) and (e) excitation of nucleon isobars, and (f) vector meson currents.

and $h_2(0)m_\pi^3 = 0.0658$, and $\gamma_p - \gamma_n$ is the difference between proton and neutron magnetic moments: $\gamma_p - \gamma_n = 4.706$ n.m.

4.3. VECTOR MESON (ρ AND ω) CURRENTS (Fig. 10f)

$$m_{\rm I} = 2\zeta_\rho \left(\frac{m_\pi}{m_\rho}\right)^3 Y_0^\rho(x), \qquad m_{\rm II} = 6\zeta_\rho \left(\frac{m_\pi}{m_\rho}\right)^3 Y_2^\rho(x),$$

$$h_{\rm I} = j_{\rm I} = \xi_\omega \left(\frac{m_\pi}{m_\omega}\right)^3 Y_0^\omega(x), \qquad h_{\rm II} = j_{\rm II} = 3\zeta_\omega \left(\frac{m_\pi}{m_\omega}\right)^3 Y_2^\omega(x),$$

where $\zeta_{\rm V}$ is a product of coupling constants, $\zeta_{\rm V} = -g_{\rm VNN}g_{{\rm V}\pi\gamma}g_{\pi{\rm NN}}/12\pi$, ${\rm V} = \rho, \omega$ such that $\zeta_\rho(m_\pi/m_\rho)^3 = -0.0056$ and $\zeta_\omega(m_\pi/m_\omega)^3 = -0.0027$. The radial functions are

$$Y_{0,2}^{\rm V}(x) = \frac{m_{\rm V}^2}{m_{\rm V}^2 - m_\pi^2}\left[Y_{0,2}(x_\pi) - \left(\frac{m_{\rm V}}{m_\pi}\right)^2 Y_{0,2}(x_{\rm V})\right],$$

where $x_{\rm V} = m_{\rm V} r$, with $m_{\rm V}$ the mass of vector meson.

Nuclear recoil and wave function orthogonalization corrections [3]) have not been calculated, as Gari and Hyuga [33]) show that in the non-relativistic limit these two corrections mutually cancel.

The computation requires the evaluation of reduced matrix elements of the operator, eq. (4), taken between antisymmetrized two-particle states. The procedure is standard: transform from *jj* to *LS* coupling and introduce c.m. and relative coordinates through the Moshinsky-Brody [34]) transformation. Oscillator functions with $\hbar\omega = 9.22$ MeV are used to evaluate the different radial integrals. Short-range correlations are approximately accommodated by using a lower cut-off at $d = 0.4$ fm in the radial integrals in the relative coordinate.

There are two types of contributions to consider. First, the situation in which one particle is in the valence space and the other in the core (this is shown diagrammatically as graph (g) in fig. 9), and second in which both particles are in the valence space (graph (h) in fig. 9). Graph (g) has the value

$$\langle j_1 \| H \| j_1 \rangle = \sum_{j_c J_1 J_2} \frac{\hat{J}_1 \hat{J}_2}{\hat{j}_1 \hat{j}_1} U(j_1 j_c 1 J_2; J_1 j_1) \langle (j_1 j_c) J_1 \| H \| (j_1 j_c) J_2 \rangle, \tag{5}$$

where $\hat{J} = (2J+1)^{\frac{1}{2}}$ and the sum j_c is over the fully occupied orbits that make up the ^{88}Sr closed shell core. This term has the appearance of an effective one-body operator in the valence space and to illustrate this further the results are re-expressed in terms of an effective magnetic moment operator $\boldsymbol{u}^{\text{eff}}$ defined as

$$\boldsymbol{u}^{\text{eff}} = \delta g_l \boldsymbol{L} + \delta g_s \boldsymbol{S} + g_p [Y_2 \times \boldsymbol{S}]^{(1)}. \tag{6}$$

The effective g-factors, δg_l, δg_s and g_p are uniquely determined by evaluating with eq. (5) the three matrix elements $\langle j_1 \| H \| j_1 \rangle$, $\langle j_2 \| H \| j_2 \rangle$ and $\langle j_1 \| H \| j_2 \rangle$ where $j_1 = l + \frac{1}{2}$ and $j_2 = l - \frac{1}{2}$ and then inverting a set of linear equations. Results are shown in table 4. It is seen that the quoted δg_l for the 1g and 2p orbitals is less than the often quoted [12,32]) empirical value of $\delta g_l \approx 0.1$. It is possible that including higher order processes, such as two-pion exchange, might enhance the calculated δg_l value [4]), but we have not investigated this point.

The meson exchange current correction to the magnetic moments of the $N = 50$ isomers are shown in rows (g) and (h) in table 3. It is seen that the core contribution, graph (g), dominates and for the isomers of a given spin, for example the three 8^+ states in ^{90}Zr, ^{92}Mo and ^{94}Ru, its contribution is the same for each as anticipated by the additivity rule for simple one-body operators. The much smaller valence contribution, graph (h), while being state dependent, has little influence on the observed 5% breakdown of the additivity rule.

Finally, we should like to draw attention to the single-particle $p_{\frac{3}{2}}$ and $p_{\frac{1}{2}}$ magnetic moments in the last two columns of table 3, and in particular to the opposite sign for their meson exchange current contribution. An examination of the operator in eq. (4) shows that it is predominantly isovector in character, only the ρ vector meson current contributes an isoscalar term and this term is small in magnitude. Secondly, in reexpressing the mesonic contribution in terms of an effective magnetic moment

TABLE 4

One-pion exchange current contribution to magnetic moments expressed as an effective operator eq. (6)

Orbit	Proton			Neutron		
	δg_l	δg_s	g_p	δg_l	δg_s	g_p
1g	0.069	0.048	0.007	−0.066	0.102	−0.041
2p	0.089	0.085	0.754	−0.058	0.135	−0.225

operator, eq. (6), it is found in most cases that the δg_l term dominates. This term derives exclusively from the translationally non-invariant portion of the pionic and pair excitation current (terms involving n_{I} and n_{II}). These observations have led to the oft-stated result that the mesonic correction to magnetic moments is positive for proton and negative for neutron states with the magnitude increasing with increasing orbital angular momentum. Thus our result that the mesonic correction for a $p_{\frac{1}{2}}$ proton state is negative requires further comment.

We find in our calculation for the p-states that the mesonic correction is predominately isovector, as anticipated, but when re-expressed in terms of the effective operator, eq. (6), the g_{p} term turns out to be larger (see table 4) than the δg_l term. As the g_{p} term gives a positive contribution for $p_{\frac{1}{2}}$ states and a negative contribution for $p_{\frac{1}{2}}$ states this accounts for our unexpected result. Furthermore, the enhancement of the g_{p} term can be traced to the nature of the ^{88}Sr closed-shell core. This core is not a closed LS core but rather has a neutron excess in orbits $p_{\frac{1}{2}}$ and $g_{\frac{1}{2}}$. On repeating our calculation with an $N = Z = 40$ closed-shell core the traditional character is restored, thus we attribute the enhancement of the g_{p} term to the role played by the neutron excess orbits. It would be interesting to see if this result can be corroborated experimentally.

5. Conclusions

The present study of g-factors in $N = 50$ isotones has revealed significant breakdowns in the additivity rule of the nuclear shell model (see fig. 8). The trend in the observed differences of g-factors is well explained by the results of first-order core polarization calculations described in the previous section. Our analysis is thus in agreement with the earlier interpretation by Nagamiya *et al.* [12]) of the g-factor results [12]) for ^{90}Zr and ^{92}Mo. An extension of the g-factor measurement to a predicted [16]) 8^+ isomer in ^{96}Pd would be valuable to corroborate this interpretation.

We have calculated the exchange current contribution to magnetic moments arising from one-pion exchange and find that its effect on the breakdown of the additivity rule is negligible. The correction mostly affects the absolute value of the g-factor and for the $N = 50$ isotones a shift of approximately $\Delta g \approx 0.06$ is calculated.

Previously, the meson exchange current contribution for these nuclei has only been estimated from a phenomenological point of view by introducing an effective magnetic moment operator, eq. (6), and adjusting the coupling constants, usually just δg_l, in a fit to the experimental data. Nagamiya *et al.* [12]) have performed such an analysis for the $N = 50$ isotones with a smaller, less accurate sample of data than that listed in table 2. Note, however, that the core polarization correction has also to be subtracted from the data before the fit can be made. Nagamiya *et al.* [12]) using a delta-function interaction to estimate this core-polarization correction, derived the result $\delta g_l = 0.10$. We have repeated the fit using in this case the experimental data from table 2 and the core polarization correction from table 3 and find that Δg_l

is not well determined ($\delta g_I \approx 0.05 \pm 0.05$). Nevertheless, it is gratifying that the result is consistent with the explicit calculation given in table 4. However, the drawback with this phenomenological approach is that the result depends sensitively on the subtraction of the core polarization contribution from the experimental data.

References

1) R. G. Sachs, Phys. Rev. **74** (1948) 433
2) H. Miyazawa, Prog. Theor. Phys. **6** (1951) 801
3) M. Chemtob and M. Rho, Nucl. Phys. **A163** (1971) 1;
   M. Chemtob, Nucl. Phys. **A123** (1969) 449
4) H. Hyuga and A. Arima, preprint
5) A: Arima and H. Horie, Prog. Theor. Phys. **11** (1954) 509;
   H. Noya, A. Arima and H. Horie, Prog. Theor. Phys. Suppl. **8** (1958) 33
6) H. A. Mavromatis, L. Zamick and G. E. Brown, Nucl. Phys. **80** (1966) 545;
   H. A. Mavromatis and L. Zamick, Nucl. Phys. **A104** (1967) 17
7) I. S. Towner, F. C. Khanna and O. Häusser, Nucl. Phys. **A277** (1977) 285
8) S. Krewald and J. Speth, Phys. Lett. **52B** (1974) 295
9) A. Richter, preprint, Technische Hochschule, Darmstadt
10) Y. Yamazaki, O. Hashimoto, H. Ikezoe, S. Nagamiya, K. Nakai and T. Yamazaki, Phys. Rev. Lett. **33** (1974) 1614
11) O. Häusser, J. R. Beene, A. B. McDonald, T. K. Alexander, E. D. Earle, F. C. Khanna, I. S. Towner, G. A. Beer and A. Olin, Phys. Lett. **63B** (1976) 279
12) S. Nagamiya, T. Katou, T. Nomura and T. Yamazaki, Phys. Lett. **33B** (1970) 574
13) B. A. Brown, P. M. S. Lesser and D. B. Fossan, Phys. Rev. Lett. **34** (1975) 161
14) J. M. Jaklevic, C. M. Lederer and J. M. Hollander, Phys. Lett. **29B** (1969) 179; Nucl. Phys. **A169** (1971) 449
15) B. A. Brown, D. B. Fossan, P. M. S. Lesser and A. R. Poletti, Phys. Rev. **C13** (1976) 1194
16) D. H. Gloeckner and F. J. D. Serduke, Nucl. Phys. **A220** (1974) 477
17) O. Häusser, T. K. Alexander, J. R. Beene, E. D. Earle, A. B. McDonald, F. C. Khanna and I. S. Towner, Nucl. Phys. **A273** (1976) 253
18) F. A. Rossini and W. D. Knight, Phys. Rev. **178** (1969) 641
19) The NBS Alloy Data Centre: Permuted Materials Index, National Bureau of Standards (US), spec. publ. no. 324 (1974);
   G. C. Carter, private communication
20) D. Riegel, Phys. Scripta **11** (1975) 228
21) J. R. Beene, O. Häusser, A. B. McDonald, T. K. Alexander, A. J. Ferguson and B. Herskind, Hyperfine Interactions **3** (1977) 397
22) F. D. Feiock and W. R. Johnson, Phys. Rev. **187** (1969) 39
23) D. C. Kocher, Nucl. Data **16** (1975) 55
24) H. J. Rose and D. M. Brink, Rev. Mod. Phys. **39** (1967) 306
25) S. Cochavi, J. M. McDonald and D. B. Fossan, Phys. Rev. **C3** (1971) 1352
26) O. Häusser, F. J. Sharp, A. B. McDonald, T. K. Alexander, J. R. Beene and R. E. Howard, Atomic Energy of Canada Limited, report AECL-5508 (1976) p. 32
27) O. Häusser, B. A. Brown, T. Faestermann, D. Ward, H. R. Andrews and D. Horn, Atomic Energy of Canada Limited, report AECL-5802 (1977), to be published
28) J. Christiansen, H. E. Mahnke, E. Recknagel, D. Riegel, G. Schatz, G. Weyer and W. Witthuhn, Phys. Rev. **C1** (1970) 613
29) A. de-Shalit and I. Talmi, Nuclear shell theory (Academic Press, NY, 1963)
30) C. Bloch and J. Horowitz, Nucl. Phys. **8** (1958) 91;
   B. H. Brandow, Rev. Mod. Phys. **39** (1967) 771;
   M. Harvey and F. C. Khanna, Nucl. Phys. **A152** (1970) 588
31) S. M. Perez, Nucl. Phys. **A136** (1969) 599
32) T. Yamazaki, T. Nomura, S. Nagamiya and T. Katou, Phys. Rev. Lett. **25** (1970) 547
33) M. Gari and H. Hyuga, Z. Phys. **A277** (1976) 291
34) T. M. Brody and M. Moshinsky, Tables of transformation brackets (Monografias del Instituto de Fisica, Mexico, 1960)